Materials Today Communications 31 (2022) 103292

Contents lists available at ScienceDirect

Materials Today Communications

journal homepage: www.elsevier.com/locate/mtcomm

A novel ZnS nanosheets-based triboelectric nanogenerator and its applications in sensing, self-powered electronics, and digital systems

Siju Mishra [a], Supraja Potu [a], Ravi Sankar Puppala [b], Rakesh Kumar Rajaboina [a], Prakash Kodali [b], Haranath Divi [a,c,*]

[a] Department of Physics, Energy Materials and Devices Lab, National Institute of Technology Warangal, 506004, India
[b] Department of Electronics and Communication Engineering, Flexible Electronics Laboratory, National Institute of Technology Warangal, 506004, India
[c] Central Research Instrumentation Facility, National Institute of Technology Warangal, 506004, India

ARTICLE INFO

Keywords:
Energy harvesting
Triboelectric nanogenerator TENG
ZnS nanosheets
Food packaging aluminium foil
Self-powered systems

ABSTRACT

The development of triboelectric nanogenerators (TENGs) based on inexpensive inorganic materials has attracted significant attention to envisage next-generation self-powered electronic devices and sensors. In this research work, the fabrication of a triboelectric nanogenerator (TENG) based on ZnS nanosheets arrays was investigated for the first time. This TENG was fabricated with ZnS nanosheets films, polydimethylsiloxane (PDMS) as active tribo-layers. The originality of this work lies in the choice of materials; pure ZnS nanosheets and PDMS-Al cover foils. By hand excitation force, the developed TENG (5 ×5 cm^2) produced an output voltage and a short-circuit current of ~8 V and ~7.12 μA respectively. In addition, the present TENG with pure ZnS nanosheets on Al substrate produced an output voltage almost twice than TENG that involved only Al substrate. In this current study, introducing ZnS nanosheets on Al substrate increased the surface area and roughness, resulting in improved performance. The study of TENG parameters confirms that the TENG (10 ×10 cm^2) with 2 cm spacing between tribo layers, applied force frequency of ~ 4–5 Hz were optimum to obtain the maximum output voltage of ~33 V. The high stability of TENG was confirmed by testing TENG response over 1000 cycles. Further, TENG was used to power portable electronic devices such as a digital watch, thermometer, calculator, and 64 LEDs when coupled to a capacitor. Finally, TENG was demonstrated for sensing force and pressure, TENG output response was used as a clock pulse for the digital circuits. The proposed TENG is easy to handle, simple and economical, and ZnS-based TENG's performance can be improved using other tribo-materials instead of PDMS.

1. Introduction

From the past decade, triboelectric nanogenerators (TENG) have attracted a lot of attention due to their innumerable applications in the fields of medical, electronics, sensors artificial intelligence e.t.c [1–4]. The TENG has been demonstrated for the conversion of various types of mechanical energies such as ocean energy, wind energy, biomechanical energy into electrical energy. Therefore, the TENG technology is considered a promising energy collection and renewable resource [5,6]. TENGs offer several benefits, including high power conversion efficiency, simple structure, low cost, durability, scalability, and ability to harvest energy from low-frequency irregular inputs energies [7,8]. The TENG is relatively a new energy collection technique that uses a combination of triboelectrification and electrostatic induction to convert mechanical energy into electricity [9]. In TENG, the periodic contact and separation between the surfaces by external mechanical strength result in electrical energy [10].

TENG includes AC to DC conversion systems and storage elements like a battery or capacitor to power up tiny electronic devices or sensors [11]. Based on electrode arrangement and polarization switch direction, four distinct modes of TENG functioning have been proposed. The four modes are vertical contact separation, lateral sliding, single electrode mode, and free-standing triboelectric layer [12,13]. Among other modes, the vertical contact separation mode has been shown for many triboelectric materials [14,15]. Therefore, we have also used the vertical contact separation procedure for our TENG operation in this manuscript.

Many portable electronic devices and sensors were operated using the power generated by TENG. However, TENG's have several drawbacks, including low power density, limited flexibility, low surface triboelectric charge density, multi-layer involvement, and complicated

* Corresponding author at: Department of Physics, Energy Materials and Devices Lab, National Institute of Technology Warangal, 506004, India.
E-mail address: haranath@nitw.ac.in (H. Divi).

https://doi.org/10.1016/j.mtcomm.2022.103292
Received 11 November 2021; Received in revised form 9 February 2022; Accepted 14 February 2022
Available online 18 February 2022

Table 1
Literature review of ZnS-based TENG's, the morphology of ZnS used, and device output voltage.

Materials	Device size	Output Performance	Type	Structure	Reference
ZnS:cu/PDMS	4×4 cm^2	27 V, 0.1 μA	Triboelectric Nanogenerator	Fabric	[26]
PDMS/ZnS:Cu	4×1.5 cm^2	126.3 V, 193.6 nA	Triboelectrification-induced electroluminescence (TIEL)	Particle	[27]
ZnS/ZnO	2×2 cm^2	156 V, 18.9 μA/cm^2	Triboelectric nanogenerator	Nanoflakes	[48]
ZnS:Cu	5×3.5 cm^2	Not available in the report	Triboelectrification-Induced Electroluminescence	Particle	[49]
ZnS/PDMS	5×5 cm^2, 10×10 cm^2	8 V, 7.12 μA, 33 V	Triboelectric Nanogenerator	Nanosheets	Current work

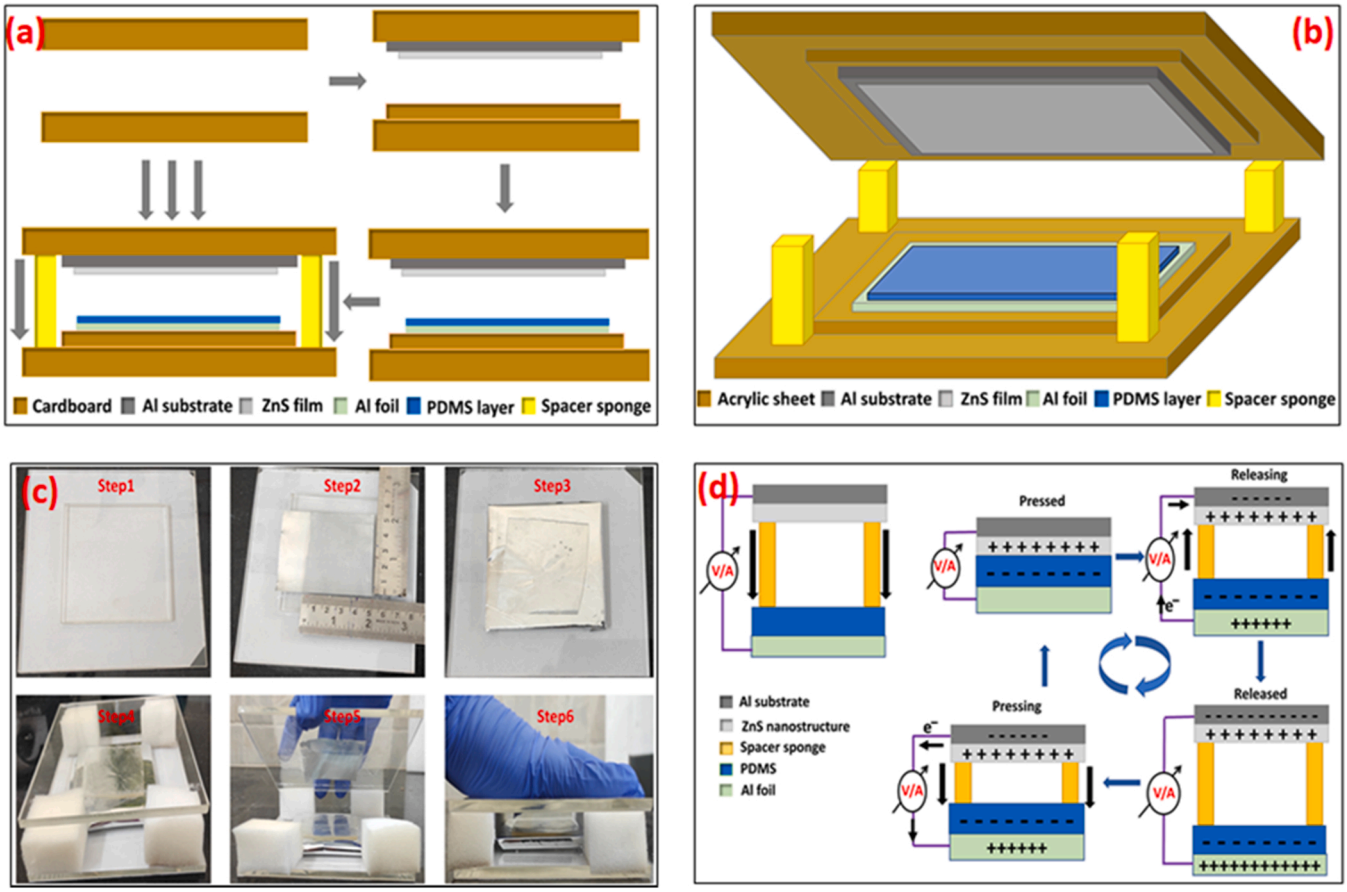

Fig. 1. (a) Fabrication of TENG schematic, (b) Fabricated TENG schematic, (c) Actual step-by-step fabrication process and, (d) TENG charge generation process.

fabrication techniques. Several approaches have been proposed in the literature to increase the power density of TENG viz. (1) increasing effective contact area or roughness [16,17], (2) various surface modification treatments [18,19], (3) cascaded TENG devices [20], (4) use of new materials as tribo-layers [21]. The surface modification, including micro/nano surface patterning into pyramids, cube lines, and nanodots, was reported to enhance TENG output. In addition, TENG output was increased with the help of treatments such as plasma etching, chemically modified nanomaterials, ionized-air injection [13,22–24]. The easy way to enhance TENG output power is to cascade a large number of TENG's. The most-reported approach to enhancing TENG output power is trying new materials and composites as an active layer for TENG. Several reports in the literature indicate that new inorganic functional materials, such as MXene (Mono transition metal), metal oxides, and sulfides and their composites, have recently been identified as promising candidates for TENG [25–27]. The performance of TENG may be considerably improved by inorganic functional materials, with strong chemical stability, high electronic conductivity, and a large surface area [28–30]. Further, TENG's were developed using different polymers such as Polyvinylidene fluoride (PVDF), Polylactic acid (PLA) [31–33]. Recently, TENG's were fabricated using bio-waste such as orange peel, fish scale, bladder, rice husk [34,35]. For wearable applications, TENG's were fabricated based on the structure and format of textiles [36,37]. The current work focuses on employing ZnS nanosheets as a new tribo material for the fabrication of TENG.

The hunt for new triboelectric couples remains a hot topic of study to increase energy efficiency and reduce TENG device cost, complexity etc. A new combination of triboelectric materials for energy harvesting applications had become the subject of recent innumerable published articles [38–40]. For the first time in the current work, intrinsic ZnS nanosheets and PDMS were used as a new triboelectric pair for mechanical energy harvesting. The aluminium substrate and waste food packaging Al cover (FPAC) foil were used as electrode materials. To the best of our knowledge, there is no report in the literature on TENG's based on pure ZnS nanosheets. However, there were few reports on ZnS-based TENG's listed in Table 1, but no one used pure ZnS and nanosheet morphology. Further, ZnS is a promising semiconducting conductor with a wide range of applications, for instance, UV nano lasers [41], micro force active sensors [42], optoelectronic devices [43], photocatalysts [44]. Although ZnS possess piezoelectric and triboelectric properties, it is not as widely explored as ZnO, $BaTiO_3$, CdSe, GaN, and PZT in nanogenerators applications. In terms of the TENG design

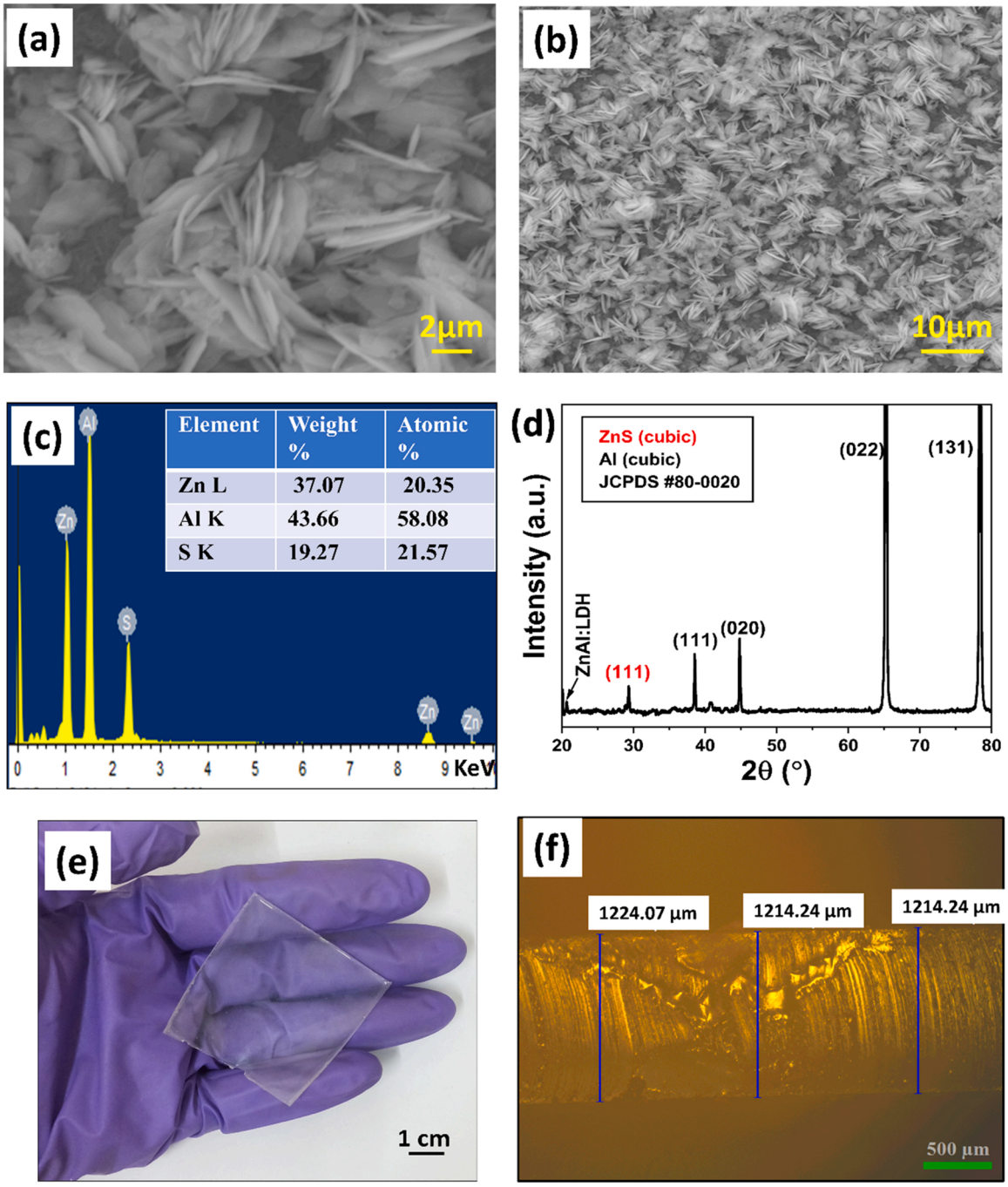

Fig. 2. (a-b) Morphology of as-synthesized ZnS film on Al substrate with different magnifications, (c) EDX spectrum of ZnS nanosheet film, (d) XRD spectra of ZnS nanosheet film, (e) Original photographs of the prepared PDMS films, (f) cross-sectional view of the PDMS using an optical microscope.

aspect, ultra-thin ZnS NSs can significantly improve the charge transfer rate between two tribo layers. The proposed ZnS-based TENG can be utilized for self-powered gas and photodetector applications in the future [45]. Further, ZnS nanosheets films selected for TENG due to their high structural stability than other nanostructure forms. Fabrication of TENG with ZnS in this manuscript has several advantages; (1) No extra electrode deposition step is required as ZnS nanosheets directly growing on the Aluminum substrate, (2) Strong adhesion of ZnS nanosheets is formed due to direct growth on the aluminum substrate, (3) no extra seed layer is required for ZnS nanosheets growth compared to the seed layer assisted ZnS nanorods/nanowires [46,47]. We have selected ZnS because of the above-said points.

The PDMS is a polymer film that is commonly used as a negative triboelectric layer for fabricating TENGs. The use of FPAC foils as electrode materials for energy harvesting substantially encourages the development of next-generation energy systems that effectively prevent pollution and risks produced by non-biodegradable materials.

For the first time, a novel TENG based on pure ZnS nanosheets on an aluminium substrate together with PDMS has been fabricated and tested for mechanical energy harvesting. Further, fabricated TENG has been demonstrated for possible applications in electronics, digital systems, and sensors.

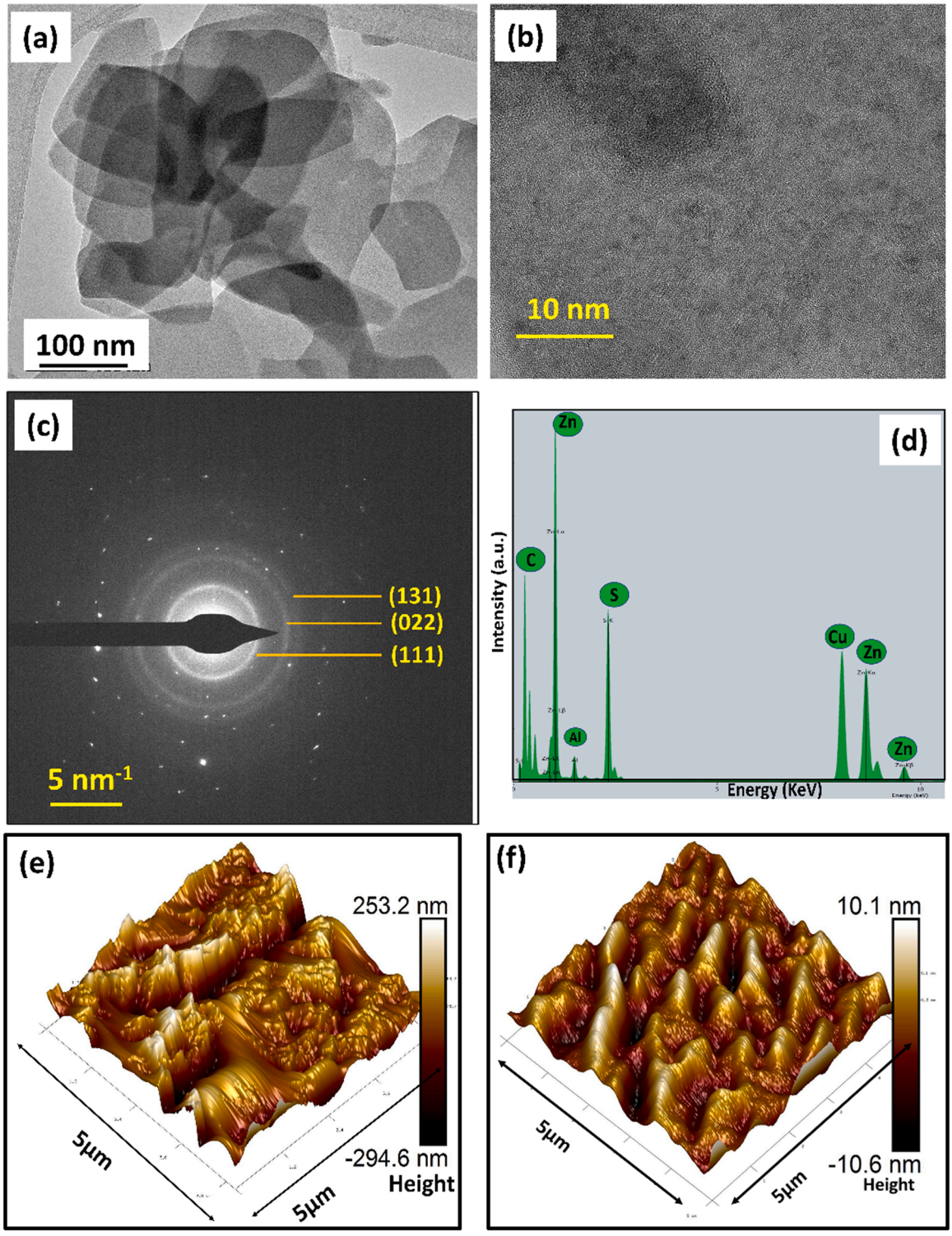

Fig. 3. (a) Transmission electron microscopy image of as-synthesized ZnS nanosheets, (b) HRTEM image of ZnS nanosheet, (c) SAED pattern recorded on ZnS nanosheet, (d) EDX spectrum collected from the single ZnS nanosheet (e) AFM image of ZnS nanosheets and, (f) AFM image of PDMS.

2. Experimental details

2.1. Materials

Zinc chloride anhydrous ($ZnCl_2$), thiourea (NH_2CSNH_2), ethylenediamine ($C_2H_4(NH_2)$) chemicals were purchased from FINAR. Acrylic sheets, Aluminum packaging foil, sponge, IC 7490, seven-segment display, and light-emitting diodes (LEDs) were brought from the local market.

2.2. Synthesis of ZnS nanosheets

The synthesis of zinc sulfide (ZnS) nanostructure is almost similar to our previous report [50]. In a typical experiment the ZnS precursor solution was made by mixing 100 mL aqueous solution of ethylenediamine (EN) (1:1 v/v) with $ZnCl_2$ and thiourea in a 1:3 molar ratio and stirred

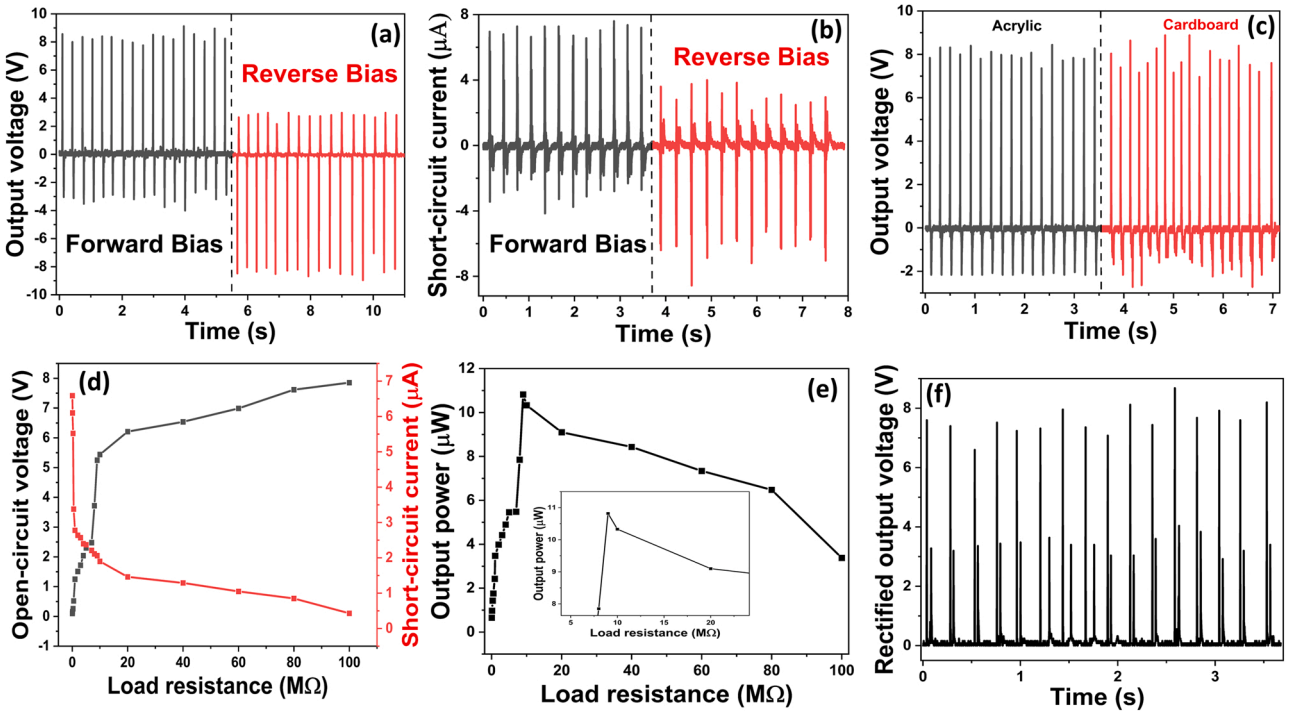

Fig. 4. (a) Forward-reverse open-circuit output voltage characteristics of TENG, (b) Forward-reverse short-circuit current of TENG, (c) Comparative output for two different bases, (d) Output voltage and current with different load resistance, (e), Output power with different load resistance, (f) Rectified output voltage using a bridge rectifier.

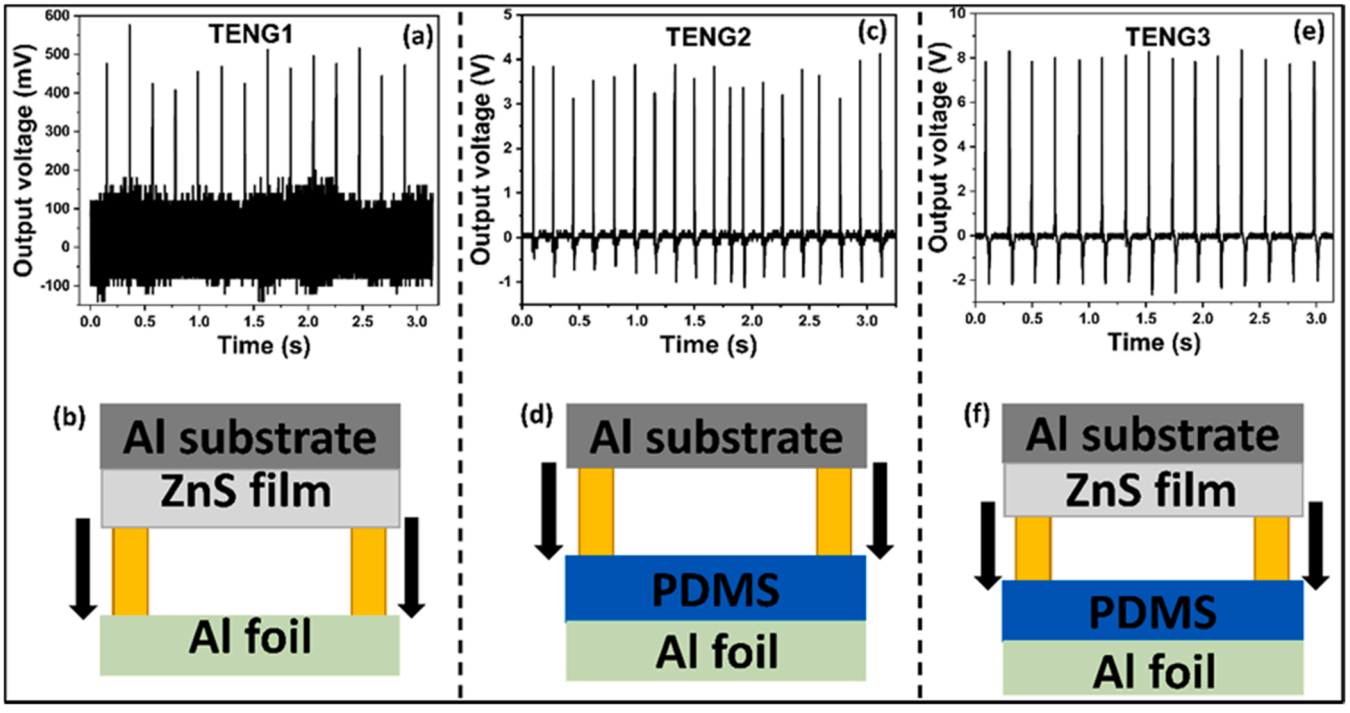

Fig. 5. (a) Output voltage of TENG1, (b) Schematic of TENG1, (c) Output voltage of TENG2, (d) Schematic of TENG2, (e) Output voltage of TENG3, (f) Schematic of TENG3.

continuously for 20 min to get a uniformly mixed solution. Further, a clean aluminium substrate (6 ×6 cm^2) was masked fully from one side with Kapton tape to avoid double side ZnS coating during synthesis. In the next step, the cleaned aluminium substrate was placed in the growth solution beaker, sealed with aluminium cover foil and transferred to the hot air oven. The synthesis of the ZnS nanosheet was performed at 160 ℃ for 4 h. The entire system was allowed to cool to room temperature naturally after the completion of the growth process. Finally, the substrates were removed from the growth solution, cleaned with de-ionized water, and dried under a hot air oven at 60 ℃. A light white-colored

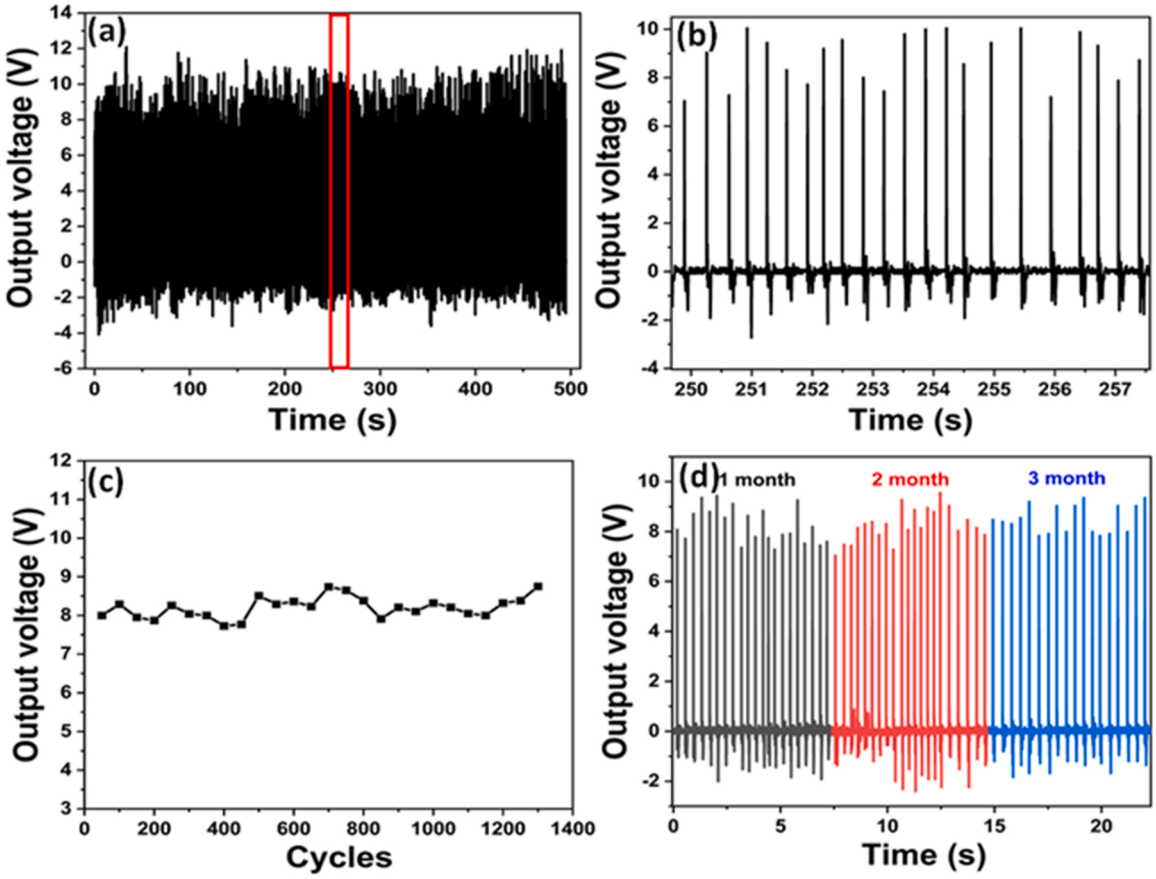

Fig. 6. (a) TENG stability under 1310 cycles, (b) Enlarged view of a few cycles of Fig. 6(a), Plot of output voltage as a function of every 50th cycles and, (d) stability of TENG over different time intervals.

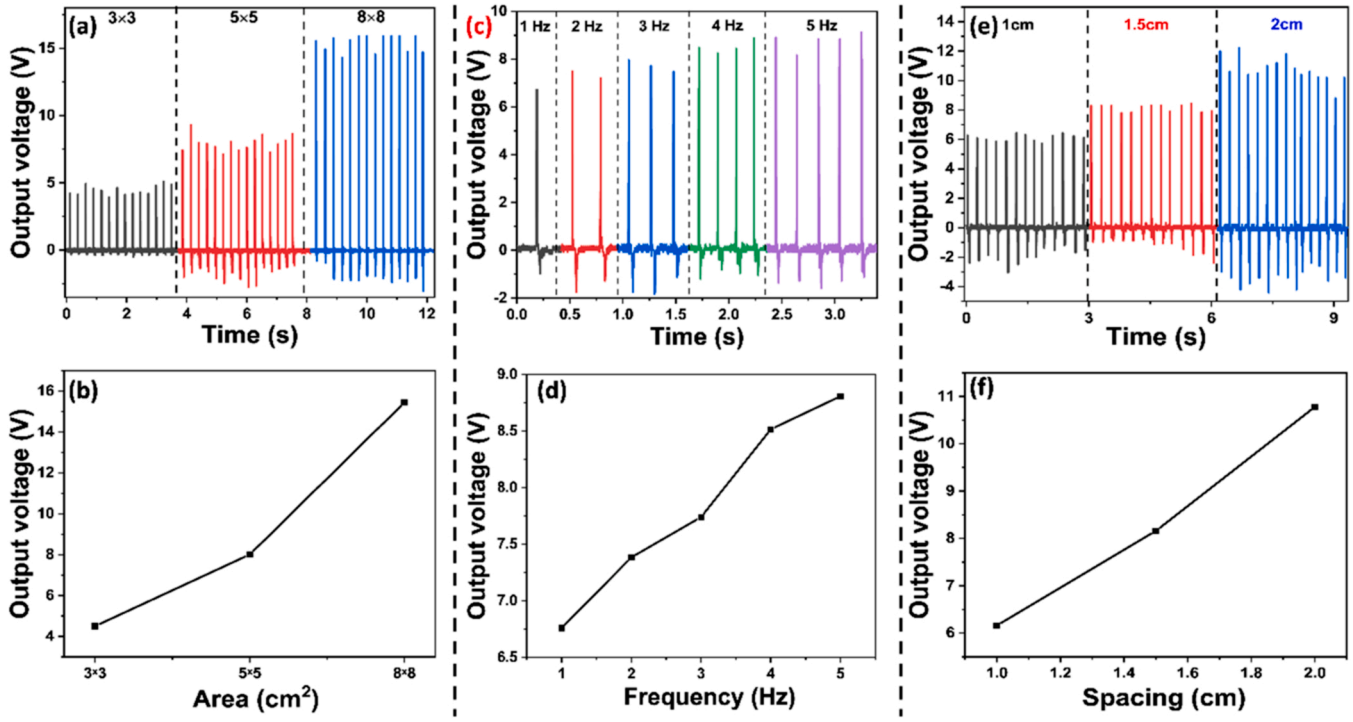

Fig. 7. (a) Comparative output of the different active area TENG's, (b) Variation of average output voltages with the different active area of TENG's, (c) Comparative output of TENG for different tapping frequency, (d) Variation of average output voltages with different tapping frequency, (e) Comparative output of TENG for different spacing between two tribo-layers, (f) Variation of average output voltages with different spacing between two tribo-layers.

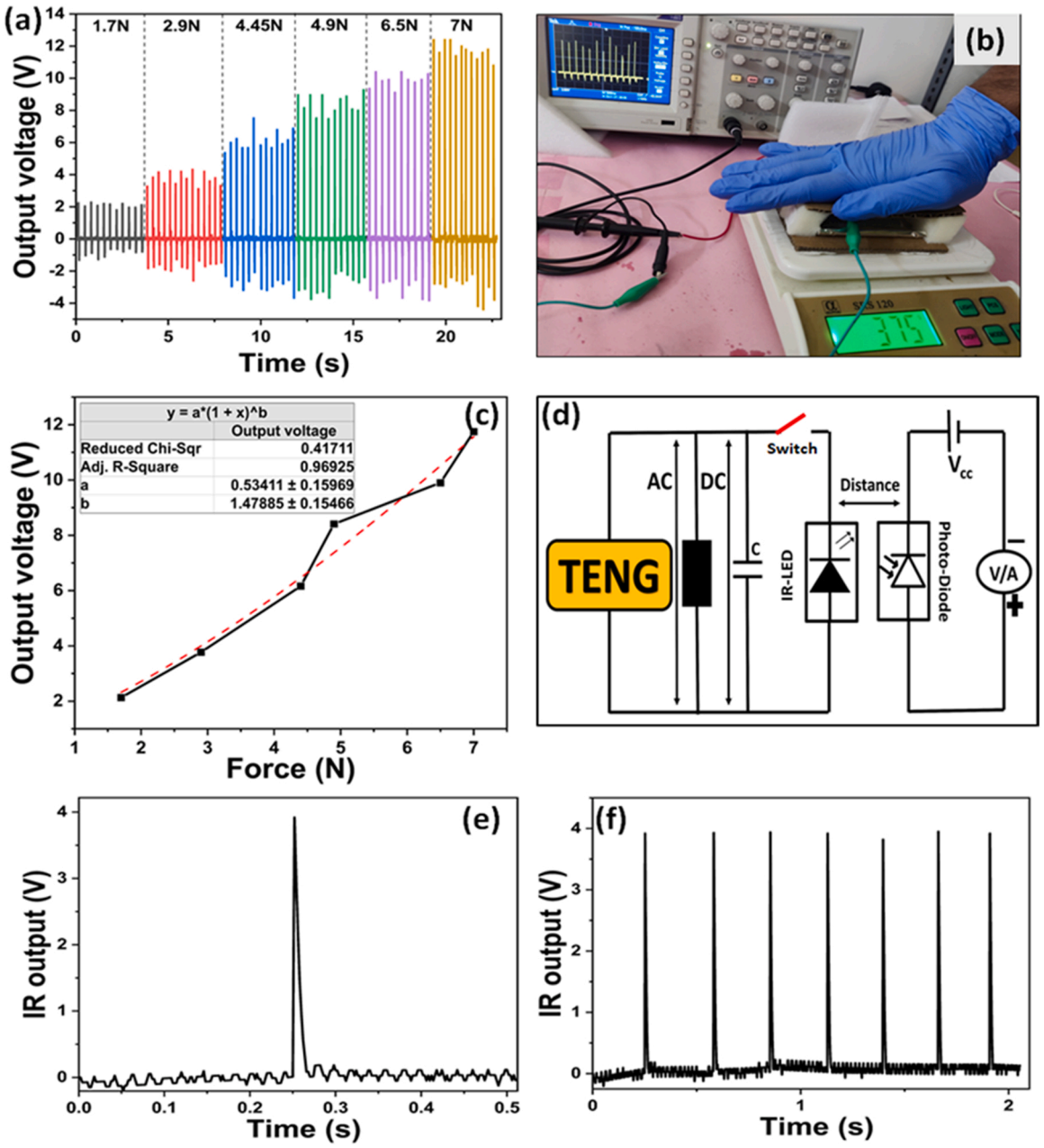

Fig. 8. (a) Output response of fabricated TENG under different applied forces, (b) Original photograph of the test setup, (c) average output voltage as a function of different applied forces and curve fitting, (d) The schematic of the circuit connections of wireless pressure/force sensing, (e) Output voltage from an IR sensor and, (f) Repeatability output of IR sensor.

uniform film was found on the Al substrate.

2.3. Preparation of PDMS films

The free-standing PDMS film of thickness ~1.2 mm was prepared by mixing base and curing agent with a weight ratio of 10:1 followed by vigorous stirring [51]. It was then put into a flat petri dish until it reached ~1.2 mm thickness and dried for about an hour in an oven at 100 ℃. A stand-alone sheet was obtained after heating, and a photograph of the PDMS sheets is shown in Fig. 2(e).

2.4. Fabrication of nanogenerator

The TENG was fabricated using ZnS nanosheets (NSs) film and PDMS as triboelectric layers in vertical contact separation mode. Initially, ZnS coated aluminium substrate with the aluminium side was firmly attached to the acrylic sheet of the selected dimension by scotch tape with ZnS nanosheets film facing up, as shown in Fig. 1(a). Similarly, Al packaging foil was attached firmly to another acrylic sheet by scotch tape with the conducting surface facing up, as shown in Fig. 1(b). Further, the PDMS sheet was attached to the bottom aluminium foil. Then, all corners of the lower acrylic sheet were attached with sponge spacers using a strong adhesive. Next, another acrylic sheet with ZnS nanosheets was placed over the spacers and attached using a strong adhesive. Due to the sponge spacer, there is a finite gap of ~1.5 cm between the upper ZnS nanosheet film and the lower PDMS surface. Fig. 1(c) shows the original photos of the constructed TENG device at different fabrication stages. Finally, two electrode lead wires were drawn from the bottom and top sides of aluminium foil and Al substrate, respectively to measure the TENG output voltage, as shown in Fig. 1(d).

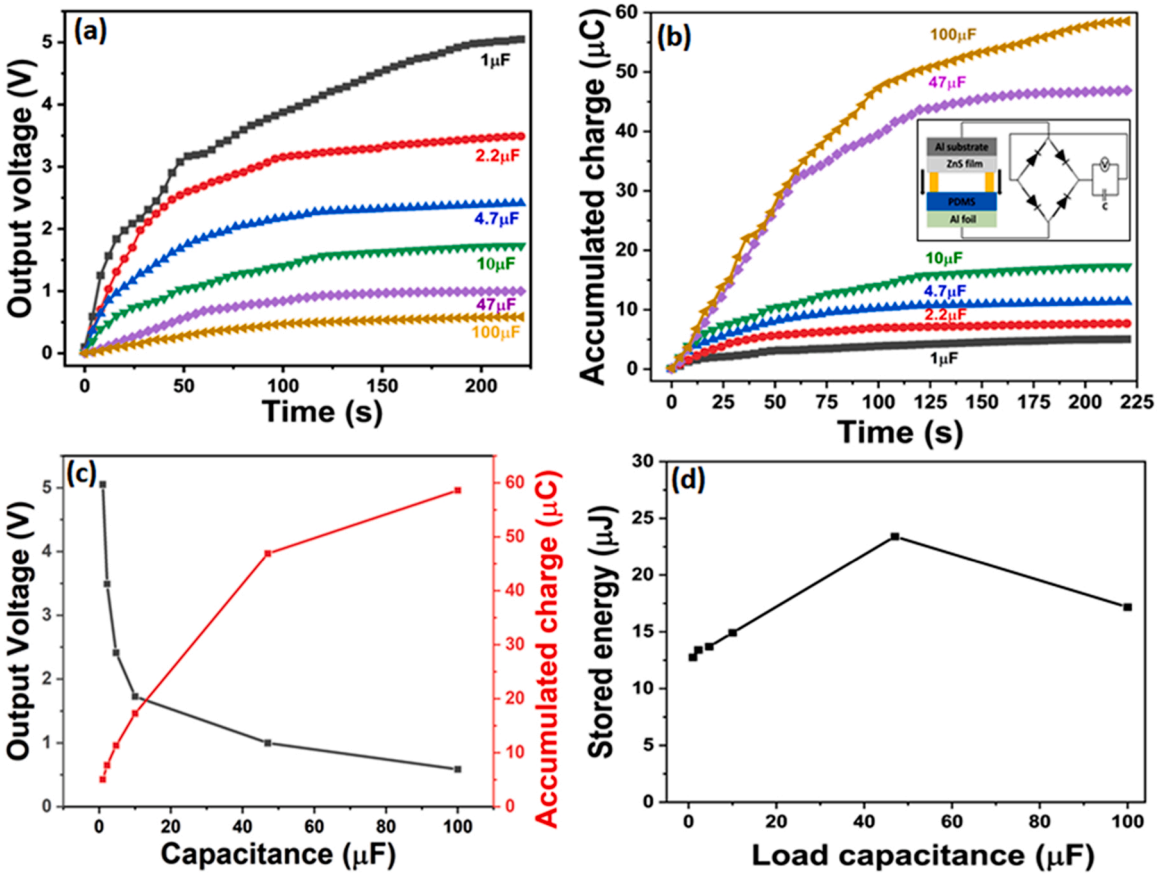

Fig. 9. (a) Charging characteristics of different capacitors with TENG, (b) Accumulated charge in different capacitors, (c) Stored charge and stored voltage behaviour of different capacitors and, (d) Stored energy in different capacitors.

2.5. Characterization techniques

A scanning electron microscope (SEM; VEGA3 TESCAN), a transmission electron microscope (TEM; JEM 200CX, JEOL), and an X-ray diffraction microscope (XRD, X-pert Pro-PW 3050/50) were used to examine the morphology, crystallinity, and compositions of the ZnS nanosheets on Al substrate respectively. Atomic force microscopy (AFM, Bruker multimode 8) technique was also used to measure the surface roughness of the ZnS nanostructure film and PDMS. The optical microscope (OLYMPUS, BX53) was used for measuring the thickness of the PDMS film. The output voltage against hand tapping was recorded using a digital oscilloscope (Tektronix TBS1102). The TENG short-circuit current was measured with an in-house-assembled current preamplifier (CNI570) [52,53]. Initially, TENG of size 5 × 5 cm^2, 1.5 cm spacing between tribo layers was characterized at a hand tapping frequency of 4 Hz. Further, the effect of the active area of tribo layers, spacing between the tribo layers, frequency of applied force, and different magnitudes of the force on the TENG output voltage were studied in detail.

3. Results and Discussion

Fig. 2(a-b) shows the morphology of the ZnS film obtained on the aluminium substrate at 160°C at two different magnifications 15000 X and 3000X, respectively. Fig. 2(a-b) confirms that the ZnS nanosheets are evenly distributed throughout the Al substrate. Further, Fig. 2(c) shows the Energy-dispersive X-ray spectroscopy (EDX) spectrum recorded from the group of nanosheets and confirms the purity of ZnS nanosheets by revealing the presence of Zn, S, and Al elements only. The crystal phase of the as-synthesized ZnS sample was further analyzed using XRD. The XRD patterns of ZnS nanostructure film are presented in Fig. 2(d). The diffraction peak at 29.32° in the XRD pattern of the ZnS NSs corresponding to the (111) plane confirms the crystalline nature of cubic ZnS (JCPDS No. #80–0020) [54]. The intense diffraction peaks at 38.59°, 44.85°, 65.24°, 78.35° in the XRD corresponding to the (111), (020), (022), (131) planes of cubic bare Al coming directly from the substrate (JCPDS No. #85–1327). The additional diffraction peaks at 20° and the corresponding (006) plan also confirms the formation of ZnAl: LDH at the interface of ZnS nanostructures and aluminium [55]. Fig. 2(e) shows the photographs of synthesized transparent PDMS film. As shown in Fig. 2(f), The PDMS film thickness was measured using an optical microscope and found to be ~1.2 mm.

Fig. 3(a) shows the transmission electron microscopy (TEM) image of ZnS nanosheets. The TEM image clearly shows that the nanosheet-like structure formed with an average width of 0.429 ± 0.015 μm, which perfectly agrees with SEM images. A typical high-resolution image of the ZnS nanosheet is shown in Fig. 3(b), and it confirms the polycrystalline nature of the sheets. In addition, the SAED pattern shown in Fig. 3(c) shows the diffraction rings that also confirms the polycrystalline nature of the ZnS nanosheets. Finally, the energy dispersive X-ray, the EDX spectrum collected from the single ZnS nanosheet is shown in Fig. 3(d), and it confirms the presence of Zn, S, Cu, C and Al elements. The elements Cu, C come from the copper grid and adsorbed carbon from the atmosphere whereas the elements Zn, S, and Al come from the ZnS nanosheets. The presence of Al may be due to the doping of ZnS nanosheets or Al particles that came along with ZnS nanosheets during TEM sample preparation. Further studies are required to confirm the doping of ZnS films.

The surface roughness of both the ZnS and PDMS surfaces were recorded using an atomic force microscope and shown in Fig. 3(e) and (f). The surface roughness values of ZnS and PDMS were found to be

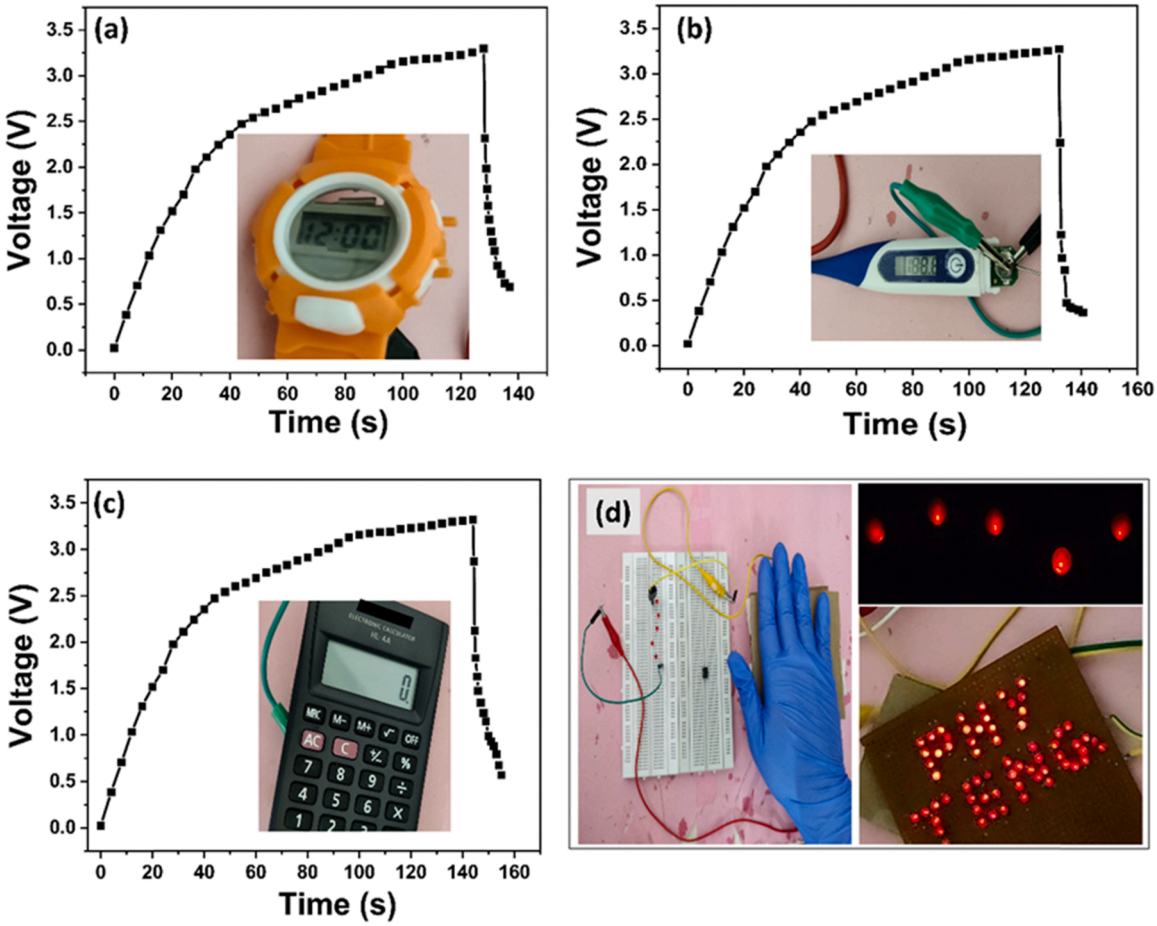

Fig. 10. (a) Charging and discharging characteristics of a 1 μF capacitor before and after power-on (a) Digital watch, (b) Digital thermometer, (c) Digital calculator and, (d) 64 LEDs glowing with the help of 1 μF capacitor and 5 LEDs glowing directly using TENG.

184 nm and 49.8 nm respectively. It is worth mentioning that the surface roughness of the ZnS film is found to be about four orders of magnitude higher than the PDMS surface roughness. This high surface roughness for ZnS thin film is attributed to the morphology of the nanosheet surface. Also, by introducing ZnS nanosheets on Al substrate the surface area increases up to 18.1% than pure Al substrate. The SEM study also well supported the AFM results of surface roughness. Furthermore, surface roughness plays a crucial role in TENG output voltage since TENG works on the principle of triboelectrification and electrostatic induction [56].

Before testing the fabricated TENG, it is necessary to analyse its functioning principle in vertical contact separation mode, which is very well discussed in the literature [57]. We have applied a similar mechanism to the present TENG in this report. The ZnS and PDMS films are connected to the upper and lower electrode layers of TENG, respectively. Each cycle of TENG generation is divided into four stages, as shown in Fig. 1(d). The TENG device is electrically neutral in the initial state because no charge is generated or inducted, with no electric potential difference between the two electrodes. Upon application of an external force on TENG, the ZnS surface gets in contact with the bottom PDMS film surface, and friction generates between them. The ZnS nanosheet film has a high degree of roughness at the nanoscale, which is due to the surface morphology, as shown in AFM Fig. 3(e). PDMS surface looks smooth at the macroscopic level; however, it will also have roughness at the nanoscale level, as shown in Fig. 3(f). Due to the friction, triboelectric layers get electrostatic charges of opposite signs, already depicted in Fig. 1(d). When both layers move apart, both electrodes get induced charges and a current flow through the load resistor from one electrode to another electrode. As a result, the device comes into balance, and no electricity passes through the circuit when both layers stop moving. Further, the current flows in the reverse direction when the external push brings two tribo layers to come closer. The repetition of these processes results in triboelectric energy [58].

Initially, TENG of dimension 5 × 5 cm^2 was tested for mechanical energy harvesting at a spacing condition between the tribolayers of 1.5 cm and frequency of applied force ~3–4 Hz. The value of the applied force was ~5 N. The open-circuit voltage of the TENG for repeated hand tapping force is shown in Fig. 4(a). An average output voltage of ~ 8 V was observed in the forward connection for the present TENG. Further, a switching polarity test was also conducted by reversing the connections of TENG and using an oscilloscope to confirm the output voltage only due to TENG operation (See SI, Video 1). Fig. 4(a) shows that the TENG showed an opposite electrical signal than the forward signal. The polarity test indicates that the voltage produced comes from TENG, not from any instrument's noise[59]. The average output voltage of ~ 8 V was observed in the reverse connection for the present TENG. Fig. 4(b) shows the average short-circuit current of ~7.12 μA for our fabricated TENG device, and current density is ~0.28 μA/cm^2 for both bias conditions. The output voltage reported in this manuscript is less than the reported literature values mentioned in Table 1. The high output voltages in those reports are due to doped ZnS and heterostructured ZnS with ZnO. In the present, manuscript we did not use any doping and heterostructure formation.

Supplementary material related to this article can be found online at doi:10.1016/j.mtcomm.2022.103292.

After a successful test of TENG with acrylic base, we have also tested our device with a cardboard base for outer structure instead of acrylic sheets base. From a cost-effective point of view, cardboard base material

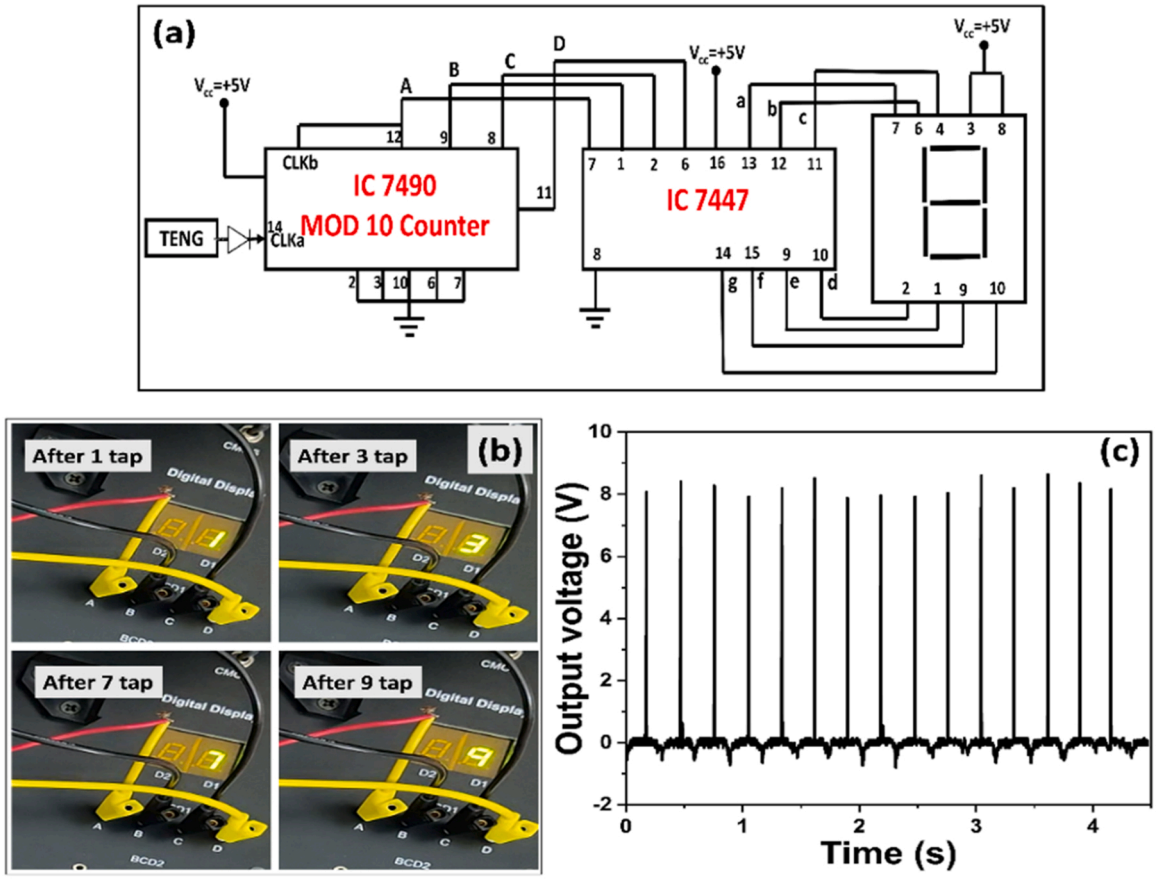

Fig. 11. (a) Schematic of decade counter circuit diagram and its connections, (b) Decimal display of counting in response to tapping and, (c) Output voltage of TENG across a half-wave rectifier.

for the fabrication of the TENG device is found to be best. The response of the TENG with different base material support is shown in Fig. 4(c), and both were giving almost the same output for 5 × 5 cm^2 area and with 3–4 Hz applied force-frequency (See SI, Video2). Therefore, we have used TENG prepared with a cardboard base was used for the remaining studies.

Supplementary material related to this article can be found online at doi:10.1016/j.mtcomm.2022.103292.

The open circuit output voltage and short-circuit current of the TENG was further measured with varying load resistances from 50 kΩ to 100 MΩ under a uniform hand tapping to find out the maximum output power. The voltage and current variation with various load resistances is shown in Fig. 4(d). With increasing load resistance, the voltage rises and saturates at ~ 7.85 V and current started from 6.588 μA at 50 kΩ load resistance and then falls up to 0.43 μA. A similar tendency is also shown in the literature for many works on TENG [60]. Z.L Wang and other research groups have suggested a simple, equivalent helpful model to understand TENG response to the load resistances [61]. The TENG is equivalent to a variable capacitor connected to a voltage source. The voltage drops across the R_L increases up to the optimum R_L and saturate at the theoretically infinite load resistance similar to open-circuit voltage. The instantaneous power output was calculated using $P = VI$ and presented in Fig. 4(e) with the varied load resistance. The highest output power of the TENG at a load resistance of 9 MΩ was 10.82 μW is shown in Fig. 4(e). Further power density was calculated by considering the active area of the device and found to be 0.433 μW/cm^2. Using the maximum power transmission theorem, the output power characteristics of the TENG device have been described. The theorem states that when the resistance value of the load is equal to the internal resistance of the source, a maximal power transfer occurs. This report shows that under impendency-matched conditions the peak power density arises [62]. Due to the saturated output voltage, the output power density was also reduced at a load resistance value above 9 MΩ. The output power behaviour of TENG with load resistance is similar to the one reported in the literature [63]. Further, the TENG output voltage was rectified to use for practical applications with the help of IC bridge rectifier DB 107. The rectified output voltage is presented in Fig. 4(f). Hence, it is proposed that TENG could be used for applications involving switching on LEDs and small electrical devices with the rectified output presented in the later section.

To understand the roles of ZnS and PDMS in TENG output voltage generation, another set of two TENG's were fabricated viz. (1) TENG1 with only ZnS nanosheets with Al foil and, (2) TENG2 with only Al substrate with PDMS. The proposed TENG with ZnS and PDMS was considered as TENG3 for comparison. The response of all TENG devices against hand tapping and their schematics are shown in Fig. 5(a-f), for TENG1, 2, and 3, respectively. The open-circuit output voltage of ~ 472 mV, ~ 3.60 V, and ~ 8.02 V were observed for TENG1, TENG2, and TENG3, respectively. After introducing ZnS nanosheets on Al substrate (TENG3), the output voltage was enhanced around 2.25 times that of a pure Al-based TENG device (TENG2). This enhancement in the TENG output can be understood from the surface roughness point of view like reported in the literature[56,64]. The TENG's output performance mainly depends on the electron affinity, the surface area, and the surface roughness of tribo layers. An increase in surface roughness effectively increases the surface area, resulting in more contact points. The TENG's output voltage effectively increases with more contact points. In the present study also, it is concluded that TENG output voltage increases with surface roughness.

It is worth mentioning that the presence of both layers (ZnS and

PDMS) in TENG3 enhanced output voltage to a greater extent. This enhancement in the output voltage is due to the tribo pairs (ZnS-Al, PDMS-Al, ZnS-PDMS) having different surface roughness and staying at different places in the triboelectric series [65].

The stability and endurance of TENG are crucial aspects for practical applications. The output voltage was measured under continuous hand tapping force for 1310 cycles and shown in Fig. 6(a) to check the durability of TENG for long-term uses. Fig. 6(a) indicates the high stability of the developed TENG because the generated voltage did not degrade after 1310 cycles. The high stability of TENG can be understood from the following explanation. We have used TENG in vertical contact separation mode. The physical damage to the tribolayers is less in this mode than other modes. The frictional layers (ZnS nanosheets and PDMS) are not undergoing any significant surface change due to friction, which results in stable (same) output voltage even after 1000 cycles. We have taken SEM images for ZnS films after 1310 cycles to support no significant surface change (See Supplementary Information SI, S1). It is clear from the SEM images that there are no substantial changes in the morphology of the ZnS nanosheets. The minor surface morphology changes did not affect the nanogenerator output voltage.

Fig. 6(b) represents the enlarged view of a few cycles from the stability graph. Further, the output voltage of every 50th cycle (for example, 50, 100, 150 and so on) was plotted and presented in Fig. 6(c). The output voltage of TENG shows an average value of 8 ± 0.5 V, and this deviation is due to the variation of hand tapping force and frequency. We have also tested our device for various time points such as one month, two months, and three months to test its repeatability outcome, and it shows almost the same output voltages in all circumstances, as shown in Fig. 6(d). The reproducibility of the results was confirmed by testing six nanogenerators fabricated under similar conditions.

To understand the TENG completely, we have studied the effect of different device sizes (active layer size), spacing between the tribo layers, and frequency of the applied force. Each parameter was studied, keeping the other two parameters constant. The response of TENG with a different area of 3×3 cm^2, 5×5 cm^2, and 8×8 cm^2 was studied at 1.5 cm spacing between tribo-layers and ~ 3–4 Hz of applied force-frequency. The response of all the three TENG's is shown in Fig. 7(a). The average output voltages of 4.50 V, 8.01 V, and 15.45 V were observed for 3×3 cm^2, 5×5 cm^2, and 8×8 cm^2 TENG devices, respectively, as shown in Fig. 7(b). The highest output voltage of ~ 15 V was observed for the device of 8×8 cm^2 area. This enhancement is due to the increased active contact area of the triboelectric layers, which is consistent with the values reported in the literature [66]. However, we have selected the device having an area of 5×5 cm^2 due to its moderate size and output for further studies. Further, we have tested the output of the TENG device (5×5 cm^2, 1.5 cm) studied at different frequencies of hand tapping force and the response shown in Fig. 7(c). The output voltage of TENG increased with frequency up to 4 Hz and then saturated above 4 Hz, as shown in Fig. 7(d). This increase in output voltage is due to the incomplete neutralization of accumulated residual charges caused by fast external tap cycles, which increase the triboelectric potential [59].

Finally, (5×5 cm^2) the response of TENG was measured as a function of the different spacing of 1 cm, 1.5 cm and, 2 cm at an applied force-frequency of ~ 3–4 Hz, and the response is shown in Fig. 7(e). The output voltage of TENG increased from 6.16 V to 10.78 V with the spacing between the tribo-layers, as shown in Fig. 7(f). The output voltage of fabricated TENG can be approximately expressed as $V_{OC} = \frac{\sigma d}{\epsilon}$, where d is the interlayer distance, σ is the surface triboelectric charge density and ϵ is the vacuum permittivity [67]. From the expression of TENG output voltage mentioned above, it is clear that the output of TENG increases with spacing between the layers. Thus, the behaviour of TENG with spacing between the layers is consistent with the reported literature [68]. Also, our fabricated TENG produced highest output voltage of ~ 33 V for 10×10 cm^2 area with 2 cm of spacing and ~ 4 Hz of applied frequency (See SI, S2, Output voltage of 10×10 cm^2 device).

Further, TENG response was recorded against different hand tapping forces, and the response of TENG was shown in Fig. 8(a). Fig. 8(b) shows the photograph of the TENG placed on a weighing balance and TENG connections to an oscilloscope. We noted the weight values on the weighing balance and the corresponding response of TENG in the oscilloscope were registered simultaneously during different applied hand tapping pressures. The force values were approximately calculated using the reported procedure in the literature [69] (See SI, S3, force calculation). Fig. 8(c) shows the variation of output voltage as a function of force. It is clear from Fig. 8(c), TENG output voltage is increasing linearly with the increase of force. The response of the TENG with different applied forces shows a similar trend as reported in the literature [16]. Therefore, the proposed TENG can be used as a force sensor if its output is calibrated against known force values. The nature of the curve is showing slightly non-linear. Hence, curve fitting was performed using Origin software to develop an equation with an output voltage as a dependent variable and force as an independent variable. To perform the non-linear fitting, Pow2P2 function i.e., $V = a(1 + F)^b$ has been used and the corresponding fitted curve was shown as red dotted line in Fig. 8 (c). The average error for every available data point was estimated to be ~6.52%. Hence one can use this formula to directly calculate the corresponding output voltage of our TENG device when a value of force is given.

In addition, TENG was demonstrated for the possible application of wireless pressure/force sensors using infrared (IR) LED and IR sensors. The schematic of the test setup is shown in Fig. 8(d). Since TENG cannot be coupled directly to IR LED, a charged capacitor is used to drive the IR LED. When the capacitor switches on the IR LED, the IR light illuminates the IR sensor at a distance of ~10 cm. As a result, the IR sensor produces an appropriate voltage in response to the light intensity, as shown in Fig. 8(e) (See SI, Video 3). The IR sensor output was tested under identical conditions of charged capacitor voltage and found a similar response, as summarized in Fig. 8(f). If the fabricated TENG could power on IR LED directly, it could be used as a wireless pressure/force sensor as well.

Supplementary material related to this article can be found online at doi:10.1016/j.mtcomm.2022.103292.

The schematic of the TENG circuit connection for charging capacitors is shown in the inset of Fig. 9(b). Various commercial capacitors such as 1 μF, 2.2 μF, 4.7 μF, 10 μF, 47 μF, 100 μF were charged with the help of TENG device for ~ 220 s and the corresponding charging curves presented in Fig. 9(a). Further, the charge stored on the load capacitors was calculated via the simple equation Q=CV. The stored charge as a time function for different load capacitors is shown in Fig. 9(b). It is well known that a capacitor with a low value of 1 μF stores a small charge and reaches the saturation state soon. Fig. 9(c) shows that the stored charge and stored voltage behaviour could be improved by increasing the capacity value. The output voltage of the 100 μF capacitor is 0.586 V, and the maximum value of the stored charges is 58.6 μC. With different load capacitance values in Fig. 9(c) indicate the characteristics of output voltage response and stored charges. The voltage and stored charges for the corresponding C_L are opposite. Fig. 9(d) demonstrates the variation of maximum stored energy with different load capacitance values. The maximum stored energy of 23.41 μJ was observed at C_L of 47 μF.

Finally, TENG was demonstrated for practical applications such as driving portable electronic devices with the help of charged capacitors. The charging and discharging curves of 2.2 μF capacitor in switching on the digital clock, calculator, thermometer, were illustrated in Fig. 10 (a)–(d) (See SI videos 4,5,6). In-set of all the Fig. 10 (a)–(c) shows the switched-on condition of portable electronic devices powered by TENG. Further, TENG was demonstrated to switch on 64 LEDs with the help of charged capacitor (1 μF) (See SI videos 7). In addition, TENG could also continuously power 5 LEDs directly by hand tapping in Fig. 10 (d) (See SI videos 8).

At last, the TENG output voltage pulse was explored as a clock pulse for the digital circuits. The circuit connections and components are presented in Fig. 11(a). IC 7490 is used as a decade counter, which counts 0–9 in response to the applied clock pulse. IC 7447 is BCD to seven segment decoders, which convert binary coded decimal (BCD) input to seven output lines. The seven output lines of IC 7447 were connected to seven segment display to display the decimal values in response to the BCD input. The BCD output of IC 7490 was connected to IC 7447, and IC 7447 output was connected to a seven-segment display. Initially, the output of TENG was allowed to pass through a diode to remove the negative part of the output signal. Fig. 11(c) shows the TENG output after passing through the diode, and this signal act as a clock for the circuit. The application of clock pulses with the output of TENG results in an increment in the counter value from zero to nine. The photographs of the different states of the counter (seven-segment display) are presented in Fig. 11(b) (See SI, Video 9).

The above experiment shows that the output of the TENG device could be used as a self-powered clock pulse generator for digital circuits as well as for any other circuits, which work using clock pulses.

4. Conclusions

In summary, a novel TENG based on the 2D ZnS nanostructure and the PDMS was developed to power tiny electronic devices and sensing applications. To the best of our knowledge, this is the first report on TENG based on ZnS nanosheets. The TENG (5×5 cm^2) device was fabricated in such a way to function in a vertical-contact separation mode and produced an output voltage and short-circuit current of ~ 8 V and 7.12 μA with a maximum power density of 0.433 μW/cm^2. Furthermore, the different device parameters such as device size, spacing between the layers, and applied force-frequency were studied. The output voltage of TENG was increased with increasing device size, frequency of applied force and spacing between the tribolayers. The TENG was demonstrated to use as a force and/or pressure sensor. Finally, The TENG was used to power portable electronic devices and LEDs. It is worth mentioning here that we have demonstrated that TENG output can be used as a clock pulse for digital circuits. This study opens up a new triboelectric pair using 2D nanostructures to gather energy. Furthermore, the fabricated TENG device may be easily scaled to large areas for improved performance. The use of food packaging aluminium cover foil and cardboard also minimizes environmental pollution to some level. It is concluded that the fabricated TENG is a promising candidate for mechanical energy harvesting and green energy sources.

CRediT authorship contribution statement

Siju Mishra: Data curation, Formal analysis, Investigation, Roles/Writing – original draft. **Supraja Potu:** Methodology, Software, Validation, Visualization. **Ravi Sankar Puppala:** Methodology, Software, Validation, Visualization. **Rakesh Kumar Rajaboina:** Resources, Funding acquisition, Supervision, Software, Writing – review & editing. **Prakash Kodali:** Supervision, Software, Software, Validation, Visualization. **Haranath Divi:** Project administration, Resources, Funding acquisition, Supervision; Writing – review & editing.

Declaration of Competing Interest

The authors declare that they have no known competing financial interests or personal relationships that could have appeared to influence the work reported in this paper.

Acknowledgments

The authors are grateful to the Central Research Instrumentation Facility (CRIF), NIT Warangal for X-ray diffraction and microscopic characterization, and Materials Research Centre (MRC), MNIT, Jaipur for extending the AFM facility. The authors are also thankful to Dr V Jayalakshmi for extending the optical microscope facility.

Appendix A. Supporting information

Supplementary data associated with this article can be found in the online version at doi:10.1016/j.mtcomm.2022.103292.

References

[1] X. Xia, Q. Liu, Y. Zhu, Y. Zi, Recent advances of triboelectric nanogenerator based applications in biomedical systems, EcoMat 2 (2020) 1–20.
[2] I. Shabbir, N. Rubab, T.W. Kim, S.W. Kim, Healthcare management applications based on triboelectric nanogenerators, APL Mater. 9 (2021) 1–14.
[3] J. Li, C. Wu, I. Dharmasena, X. Ni, Z. Wang, H. Shen, S.-L. Huang, W. Ding, Triboelectric nanogenerators enabled internet of things: a survey, Intell. Converg. Netw. 1 (2020) 115–141.
[4] Y. Zhou, M. Shen, X. Cui, Y. Shao, L. Li, Y. Zhang, Triboelectric nanogenerator based self-powered sensor for artificial intelligence, Nano Energy 84 (2021), 105887.
[5] R. Yu, W. Wu, Y. Ding, Z.L. Wang, GaN nanobelt-based strain-gated piezotronic logic devices and computation, ACS Nano 7 (2013) 6403–6409.
[6] Z.L. Wang, J. Song, Piezoelectric nanogenerators based on zinc oxide nanowire arrays, Science 312 (2006) 242–246.
[7] P. Bai, G. Zhu, Z.H. Lin, Q. Jing, J. Chen, G. Zhang, J. Ma, Z.L. Wang, Integrated multilayered triboelectric nanogenerator for harvesting biomechanical energy from human motions, ACS Nano 7 (2013) 3713–3719.
[8] M. Lee, C.Y. Chen, S. Wang, S.N. Cha, Y.J. Park, J.M. Kim, L.J. Chou, Z.L. Wang, A hybrid piezoelectric structure for wearable nanogenerators, Adv. Mater. 24 (2012) 1759–1764.
[9] Z.L. Wang, On Maxwell's displacement current for energy and sensors: the origin of nanogenerators, Mater. Today 20 (2017) 74–82.
[10] S. Pan, Z. Zhang, Fundamental theories and basic principles of triboelectric effect: a review, Friction 7 (2019) 2–17.
[11] S.S.K. Mallineni, H. Behlow, Y. Dong, S. Bhattacharya, A.M. Rao, R. Podila, Facile and robust triboelectric nanogenerators assembled using off-the-shelf materials, Nano Energy 35 (2017) 263–270.
[12] Z. Lin, J. Chen, J. Yang, J. Nanomater 2016 (2016).
[13] C. Wu, A.C. Wang, W. Ding, H. Guo, Z.L. Wang, Hybrid supercapacitors: an aqueous zn-ion hybrid supercapacitor with high energy density and ultrastability up to 80 000 cycles, Adv. Energy Mater. 9 (2019) 1–25.
[14] J. Shao, M. Willatzen, Z.L. Wang, J. Appl. Phys. 128 (2020).
[15] B. Yang, W. Zeng, Z.H. Peng, S.R. Liu, K. Chen, X.M. Tao, Li-Ion batteries: suppressing Fe-Li antisite defects in $LiFePO_4$/carbon hybrid microtube to enhance the lithium ion storage, Adv. Energy Mater. 6 (2016) 1–8.
[16] J. Chun, B.U. Ye, J.W. Lee, D. Choi, C.Y. Kang, S.W. Kim, Z.L. Wang, J.M. Baik, The intestinal copper exporter CUA-1 is required for systemic copper homeostasis in caenorhabditis elegans, Nat. Commun. 7 (2016) 1–9.
[17] C.K. Chung, K.H. Ke, The association between trauma centrality and posttraumatic stress among syrian refugees: the impact of cognitive distortions and trauma-coping self-efficacy, J. Interpers. Violence 508 (2020) 1852–1877.
[18] M. Muthu, R. Pandey, X. Wang, A. Chandrasekhar, I.A. Palani, V. Singh, Enhancement of triboelectric nanogenerator output performance by laser 3D-Surface pattern method for energy harvesting application, Nano Energy 78 (2020), 105205.
[19] T. Prada, V. Harnchana, A. Lakhonchai, A. Chingsungnoen, Comparing the medicaid prospective drug utilization review program cost-savings methods used by state agencies in 2015 and 2016, Am. Health Drug Benefits 12 (2019) 7–12.
[20] L. Xu, T. Jiang, P. Lin, J.J. Shao, C. He, W. Zhong, X.Y. Chen, Z.L. Wang, Coupled triboelectric nanogenerator networks for efficient water wave energy harvesting, ACS Nano 12 (2018) 1849–1858.
[21] H. Liu, H. Wang, Y. Lyu, C. He, Z. Liu, A novel triboelectric nanogenerator based on carbon fiber reinforced composite lamina and as a self-powered displacement sensor, Microelectron. Eng. 224 (2020), 111231.
[22] Y. Yang, H. Zhang, Z.L. Wang, Direct-current triboelectric generator, Adv. Funct. Mater. 24 (2014) 3745–3750.
[23] Y. Qian, M. Sohn, W. He, H. Park, K.R.V. Subramanian, D.J. Kang, A high-output flexible triboelectric nanogenerator based on polydimethylsiloxane/three-dimensional bilayer graphene/carbon cloth composites, J. Mater. Chem. A 8 (2020) 17150–17155.
[24] W. Ma, J. Lu, B. Wan, D. Peng, Q. Xu, G. Hu, Y. Peng, C. Pan, Z.L. Wang, Adv. Mater. 32 (2020) 1–9.
[25] D. Wang, Y. Lin, D. Hu, P. Jiang, X. Huang, Multifunctional 3D-MXene/PDMS nanocomposites for electrical, thermal and triboelectric applications, Compos. Part A Appl. Sci. Manuf. 130 (2020), 105754.
[26] M. He, W. Du, Y. Feng, S. Li, W. Wang, X. Zhang, A. Yu, L. Wan, J. Zhai, Flexible and stretchable triboelectric nanogenerator fabric for biomechanical energy harvesting and self-powered dual-mode human motion monitoring, Nano Energy 86 (2021), 106058.
[27] J. Li, Z. Zhang, X. Luo, L. Zhu, Z.L. Wang, Triboelectric leakage-field-induced electroluminescence based on ZnS:Cu, ACS Appl. Mater. Interfaces 14 (2022) 4775–4782.

[28] Y. Yang, J. Qi, Q. Liao, Y. Zhang, L. Tang, Z. Qin, Synthesis and characterization of Sb-doped ZnO nanobelts with single-side zigzag boundaries, J. Phys. Chem. C 112 (2008) 17916–17919.
[29] Y. Zheng, S. Zheng, H. Xue, H. Pang, Adv. Funct. Mater. 28 (2018) 1–28.
[30] L. Zheng, F. Teng, X. Ye, H. Zheng, X. Fang, Adv. Energy Mater. 10 (2020) 1–32.
[31] D. Lopez, A.R. Chowdhury, A.M. Abdullah, M. Ul, K. Sadaf, I. Martinez, B.D. Choudhury, S. Danti, C.J. Ellison, K. Lozano, M.J. Uddin, Polymer based triboelectric nanogenerator for cost- effective green energy generation and implementation of surface-charge engineering, 2001088 (2021) 1–9.
[32] R. Pan, W. Xuan, J. Chen, S. Dong, H. Jin, X. Wang, Fully biodegradable triboelectric nanogenerators based on electrospun polylactic acid and nanostructured gelatin films, Nano Energy 45 (2018) 193–202.
[33] T. Bhatta, P. Maharjan, H. Cho, C. Park, S.H. Yoon, S. Sharma, M. Salauddin, M. T. Rahman, S.M.S. Rana, J.Y. Park, High-performance triboelectric nanogenerator based on MXene functionalized polyvinylidene fluoride composite nanofibers, Nano Energy 81 (2021), 105670.
[34] R.A. Shaukat, Q.M. Saqib, M.U. Khan, M.Y. Chougale, J. Bae, Bio-waste sunflower husks powder based recycled triboelectric nanogenerator for energy harvesting, Energy Rep. 7 (2021) 724–731.
[35] Q.M. Saqib, R.A. Shaukat, M.U. Khan, M. Chougale, J. Bae, Biowaste peanut shell powder-based triboelectric nanogenerator for biomechanical energy scavenging and sustainably powering electronic supplies, *ACS Appl. Electron. Mater.* 2, 12, (2020) 3953–3963.
[36] Y. Jao, P. Yang, C. Chiu, Y. Lin, S. Chen, A textile-based triboelectric nanogenerator with humidity-resistant output characteristic and its applications in self-powered healthcare sensors, Nano Energy 50 (2018) 513–520.
[37] W. Sangkhun, Natural textile based triboelectric nanogenerators for efficient energy harvesting applications, Nanoscale 4 (2021) 2420–2428.
[38] Y. Hu, Z. Zheng, Progress in textile-based triboelectric nanogenerators for smart fabrics, Nano Energy 56 (2019) 16–24.
[39] R. Zhang, H. Olin, Material choices for triboelectric nanogenerators: a critical review, EcoMat 2 (2020) 1–13.
[40] S. Chao, H. Ouyang, D. Jiang, Y. Fan, Z. Li, Triboelectric nanogenerator based on degradable materials, EcoMat 3 (2021) 1–19.
[41] Q. Xiong, G. Chen, J.D. Acord, X. Liu, J.J. Zengel, H.R. Gutierrez, J.M. Redwing, L. C. Lew Yan Voon, B. Lassen, P.C. Eklund, Optical properties of rectangular cross-sectional ZnS nanowires, Nano Lett. 4 (2004) 1663–1668.
[42] J.M. Wu, C.C. Kao, Self-powered pendulum and micro-force active sensors based on a ZnS nanogenerator, RSC Adv. 4 (2014) 13882–13887.
[43] B.Y. Geng, X.W. Liu, Q.B. Du, X.W. Wei, L.D. Zhang, Structure and optical properties of periodically twinned ZnS nanowires, Appl. Phys. Lett. 88 (2006) 16–19.
[44] Z. Fang, S. Weng, X. Ye, W. Feng, Z. Zheng, M. Lu, S. Lin, X. Fu, P. Liu, Defect engineering and phase junction architecture of wide-bandgap ZnS for conflicting visible light activity in photocatalytic h_2 evolution, ACS Appl. Mater. Interfaces 7 (2015) 13915–13924.
[45] X. Wang, Z. Xie, H. Huang, Z. Liu, D. Chen, G. Shen, Gas sensors, thermistor and photodetector based on ZnS nanowires, J. Mater. Chem. 22 (2012) 6845–6850.
[46] Z.L. Wang, Zinc oxide nanostructures: Growth, properties and applications, J. Phys. Condens. Matter 16 (2004) 9201–9208.
[47] C. Wang, J. Li, W. Feng, Y. Ye, H. Guo, Effect of seed layer on structure and luminescence properties of ZnS nanostructures, Optics 242 (2021), 167095.
[48] Y. Qian, J. Yu, F. Zhang, Y. Kang, C. Su, H. Pang, Facile synthesis of sub-10 nm ZnS/ZnO nanoflakes for high-performance flexible triboelectric nanogenerators, Nano Energy 88 (2021), 106256.
[49] Y. Chen, X. Wei, H. Li, Y. Fan, W. Hu, G. Zhu, Stretchable hybrid bilayered luminescent composite based on the combination of strain-induced and triboelectrification-induced electroluminescence, ACS Omega 4 (2019) 20470–20475.
[50] S. Mishra, P. Supraja, P.R. Sankar, R.R. Kumar, K. Prakash, D. Haranath, Controlled synthesis of luminescent ZnS nanosheets with high piezoelectric performance for designing mechanical energy harvesting device, Mater. Chem. Phys. 277 (2022), 125264.
[51] J. Wang, S. Qian, J. Yu, Q. Zhang, Z. Yuan, S. Sang, X. Zhou, L. Sun, The flexible lubrication performance of graphene used in diamond interface as a solid lubricant: first-principles calculations, Nanomaterials 9 (2019) 1784.
[52] S.S.K. Mallineni, H. Behlow, R. Podila, A.M. Rao, A low-cost approach for measuring electrical load currents in triboelectric nanogenerators, Nanotechnol. Rev. 7 (2018) 149–156.
[53] A. Sharma, P. Agarwal, Triboelectric energy harvester performance enhanced by modifying the tribo-layer with cost-effective fabrication, Mater. Res. Express 6 (2019), 065514.
[54] S. Khan, J.S. Han, S.Y. Lee, S.H. Cho, ZnS nano-spheres formed by the aggregation of small crystallites and their photocatalytic degradation of eosin B, Chin. J. Chem. 35 (2017) 159–164.
[55] V. Gaddam, R.R. Kumar, M. Parmar, G.R.K. Yaddanapudi, M.M. Nayak, K. Rajanna, Morphology controlled synthesis of Al doped ZnO nanosheets on Al alloy substrate by low-temperature solution growth method, RSC Adv. 5 (2015) 13519–13524.
[56] V. Vivekananthan, A. Chandrasekhar, N.R. Alluri, Y. Purusothaman, S.J. Kim, A highly reliable, impervious and sustainable triboelectric nanogenerator as a zero-power consuming active pressure sensor, Nanoscale Adv. 2 (2020) 746–754.
[57] S. Rathore, S. Sharma, B.P. Swain, R.K. Ghadai, A critical review on triboelectric nanogenerator, IOP Conf. Ser. Mater. Sci. Eng. 377 (2018), 012186.
[58] Y.P. Jeon, C. Wu, K.H. Yoo, T.W. Kim, Enhancement of the output voltage for triboelectric nanogenerators due to Al doping in the zinc oxide layer, J. Alloy. Compd. 831 (2020), 154913.
[59] F.R. Fan, Z.Q. Tian, Z. Lin Wang, Flexible triboelectric generator, Nano Energy 1 (2012) 328–334.
[60] K. Xia, Z. Zhu, H. Zhang, Z. Xu, A triboelectric nanogenerator as self-powered temperature sensor based on PVDF and PTFE, Appl. Phys. A Mater. Sci. Process. 124 (2018) 0.
[61] S. Niu, Y. Liu, Y.S. Zhou, S. Wang, L. Lin, Z.L. Wang, Optimization of triboelectric nanogenerator charging systems for efficient energy harvesting and storage, IEEE Trans. Electron Devices 62 (2015) 641–647.
[62] J. Bird, Electrical circuit theory and technology, Electr. Circuit Theory Technol. (2003).
[63] V. Vivekananthan, W.J. Kim, N.R. Alluri, Y. Purusothaman, K.S. Abisegapriyan, S. J. Kim, A sliding mode contact electrification based triboelectric-electromagnetic hybrid generator for small-scale biomechanical energy harvesting, Micro Nano Syst. Lett. 7 (2019) 0–7.
[64] T. Prada, V. Harnchana, A. Lakhonchai, A. Chingsungnoen, P. Poolcharuansin, N. Chanlek, A. Klamchuen, P. Thongbai, V. Amornkitbamrung, Enhancement of output power density in a modified polytetrafluoroethylene surface using a sequential O2/Ar plasma etching for triboelectric nanogenerator applications, Nano Res. 15 (2022) 272–279.
[65] M.A. Parvez Mahmud, N. Huda, S.H. Farjana, M. Asadnia, C. Lang, Recent advances in nanogenerator-driven self-powered implantable biomedical devices, Adv. Energy Mater. 8 (2018), 1701210.
[66] Q. Wang, M. Chen, W. Li, Z. Li, Y. Chen, Y. Zhai, Size effect on the output of a miniaturized triboelectric nanogenerator based on superimposed electrode layers, Nano Energy 41 (2017) 128–138.
[67] S. Niu, Z.L. Wang, Theoretical systems of triboelectric nanogenerators, Nano Energy 14 (2014) 161–192.
[68] P.R. Sankar, K. Prakash, P. Supraja, R. Rakesh Kumar, S. Mishra, D. Haranath, A triboelectric nanogenerator based on food packaging Aluminium foil and Parafilm for self-powered electronics, Phys. Scr. 96 (2021), 125005.
[69] A. Sultana, M.M. Alam, S. Garain, T.K. Sinha, T.R. Middya, D. Mandal, An effective electrical throughput from PANI supplement ZnS nanorods and PDMS-based flexible piezoelectric nanogenerator for power up portable electronic devices: an alternative of MWCNT filler, ACS Appl. Mater. Interfaces 7 (2015) 19091–19097.